RSC Advances

This article can be cited before page numbers have been issued, to do this please use: A. Krishnan, T. S. Sreeremya and S. Ghosh, *RSC Adv.*, 2016, DOI: 10.1039/C6RA07504E.

ROYAL SOCIETY OF CHEMISTRY

www.rsc.org/advances

View Article Online
DOI: 10.1039/C6RA07504E

Journal Name

ARTICLE

Size-Tuned Hydrophilic Cerium oxide Nanoparticles as a 'Turn-on' Fluorescent Sensor for the Rapid Detection of Ultralow Concentration Vitamin C

Received 00th March 20xx,
Accepted 00th May 20xx

DOI: 10.1039/x0xx00000x

www.rsc.org/

Asha Krishnan,[a] Thadathil S. Sreeremya[a] and Swapankumar Ghosh*[ab]

The novel perspective of cerium dioxide as a fluorescent sensor has been demonstrated in the present study. The green coloured emission associated with the nanodimension of ceria has been adopted as an analytical tool to sense vitamin C, which is a biologically important molecule, in its dilute solution. Ultra fine ceria nanoparticles of average size 2.2 nm have been fabricated by a surfactant assisted thermal decomposition strategy. The particular fashion of attachment of the surfactant, oleic acid with ceria resulted in the surface hydrophobicity of the nanoparticle which in turn prevents its interaction with a hydrophilic molecule like vitamin C in the reaction media. In order to tackle the incompatibility of the nanoparticles with water, a hydrophilic surfactant coating has been grafted over its surface via bilayer surface fictionalisation. The success in the accomplished scheme has been confirmed by thermogravimetric analyses, zeta potential and contact angle measurements. The redox property of ceria and its influence on the optical properties served as a yardstick to quantify vitamin C in the concentration range 10^{-7}–10^{-4} M with a much lower value of the limit of detection (LoD) of 500 nM. The designed sensor exhibits a rapid 'turn on' fluorescence response within 30 seconds and the reversibility of fluorescence even after 5 cycles of vitamin C addition corroborates its reusability. The high selectivity of the method to detect vitamin C again point up its suitable candidature as an analytical tool. The realistic application of the sensor has also been displayed by the quantification of vitamin C in pharmaceutical formulations within agreeable error limits.

Introduction

In the light of recent advances in science and technology, there is an urge to discover innovative materials as well as to ameliorate existing functionalities capable of imparting a scientific revolution. In this aspect, exploring the obscured applications of current materials beyond their conventional uses is a hot topic of current research. Nanosized cerium dioxide or ceria is a functionally esteemed semiconductor employed for plentiful synchronised applications by virtue of their characteristic features like high thermal and chemical stability, redox nature, oxygen storage capacity and other tuneable physiochemical properties.[1–4] Ceria crystallises in the face centered cubic fluorite mode with a Fm3m crystal structure in which Ce^{4+} cations occupy the cubic corner, which is in turn coordinated to O^{2-} ions present in the tetrahedral voids.[5] Besides Ce^{4+}, cerium ions also exist as Ce^{3+} in the crystal phase of ceria, owing to the lower interconversion energy between the two oxidation states[6] and thus there is an ease of formation of oxygen vacancies in the crystal. In fact, mainstream of the accomplished utility of ceria is due to its redox property, which is bestowed by the lattice oxygen vacancies. With respect to this unique redox property, ceria has been traditionally exploited as an automobile exhaust catalyst, anti-oxidant agent, in solid oxide fuel cells (SOFC), as an oxygen gas sensor, in oxygen permeation membrane systems, as catalysts for reactions involving oxidation etc.[7-10]

The foremost enthralment of the redox property of ceria is its tenability with the Ce^{3+} to Ce^{4+} ratio in the crystal. With reference to literature, both size as well as morphology of ceria nanostructures is the paramount factor which determines the amount of Ce^{3+} present in the crystal facets.[5,11] As of the size of the crystal, reduction in overall dimension of moiety favours higher Ce^{3+} to Ce^{4+} ratio in connection with the high surface to volume ratio. Deshpande et al. observed a 15% increase in Ce^{3+} concentration when the particle size was decreased from 6 nm to 3 nm.[5] Lee et al. demonstrated that the anti-oxidant property as well as the ROS scavenging ability of ceria nanoparticles is a function of the crystal diameter.[12] For crystals with unique morphology, the oxygen vacancy concurrently varies with the exposed crystal planes resulted from the alignment and growth of crystals under the prevailed synthetic conditions.[13] In accordance with previous studies, ceria nanostructures with exposed (100) and (111) crystal facets posses higher oxygen storage

[a] Functional Materials Section (MSTD), National Institute for Interdisciplinary Science & Technology (NIIST), Council of Scientific & Industrial Research (CSIR), Trivandrum-695019, India.
[b] Project Management Division, CSIR-Central Glass & Ceramic Research Institute, 196 Raja S. C. Mullick Road, Kolkata-700 032, India, E-mail: swapankumar.ghosh2@mail.dcu.ie; ashakarthika7@yahoo.co.in; Fax: +91 33 24730957; Tel: +91 33 23223546

†Electronic Supplementary Information (ESI) available: See DOI: 10.1039/x0xx00000x

View Article Online
DOI: 10.1039/C6RA07504E

capacity and hence offers better catalytic activity.[14] Studies by our group also implied that ceria nanostructures with a mixed morphology of rods and cubes showed higher activity towards the combustion of diesel soot owing to the higher texture co-efficient of exposed active planes.[13] In short, ceria is endowed with a tunable redox centre, possessing futuristic scope for pragmatic applications. Apart from the customary uses, there are few secluded footsteps towards the utility of ceria for distinct applications which are countable in number. Hirst et al. revealed the anti-inflammatory properties of ceria nanoparticles by means of their ability to scavenge nitric oxide (NO) free radicals, the critical mediator of inflammation.[15] Ceria based hierarchical mesoporous structure fabricated by Corma et al. exhibited linear photovoltaic response, offering its candidature as a photoactive semiconductor for the construction of solar–cells.[16] Patil et al. designed ceria as a drug carrier for transport and releasing Human carbonic anhydrase (hCAII) inhibitors which are capable of controlling glaucoma, a medical condition causing blindness.[17] Inverse opal 3DOM ceria films engineered by Waterhouse et al. using a colloidal crystal template approach, exhibited photonic band gaps in the visible region, suggesting its application as an optical sensor.[18] Suresh babu et al. tuned ceria as a strong upconversion material capable of killing lung cancer cells and projected its versatility as an anti–cancer agent.[19] On account of the superoxide dismutase (SOD) mimetic activity of ceria, there are also few reports on its potential for medical and therapeutic applications.[20] Besides, ceria has also been explored as sensors for the determination of various chemical moieties which are tagged as either detrimental or indispensable stuffs.[21-26] With reference to recent literatures on ceria, it could be accounted that efforts are still in progress to unveil the concealed aspects of ceria so as to widen its technological and commercial importance.

On the subject of the impact of nanotechnology in ceria based research, there have been numerous adoptable synthetic strategies for nanoscale ceria which could successfully fabricate crystals with dimension as fine as 1.8 nm.[27] The green coloured emission exhibited by ceria with respect to its diminutive dimension, owing to the augmented Ce^{3+} concentration further accentuates its versatility as a new generation material.[28] In the present context, ceria had been designed as a fluorescent sensing probe for the detection of vitamin C, based on the size induced green emission and its dependence on the Ce^{3+} content. Vitamin C or ascorbic acid is a biologically imperative molecule assigned with multifunctional roles in human beings like metabolism, neurotransmission, nutrition, immunisation, electron transport, wound healing etc.[29-31] Human body is not able to synthesise vitamin C and consequently it has to be provided externally through diet, unless, its deficiency causes serious disorders like scurvy, gingival bleeding etc.[30] Due to its medical relevance, there have been plenty pharmaceutical supplements for vitamin C and as it is prone to easy degradation,[32] accurate quantification of these molecules in their supplements is vital to assure the quality. Many analytical techniques have been developed so far towards this goal including electrochemical, spectrophotometric and chromatographic methods, each of them having their own flaws and faults.[31,33,34] Although many of these methods are capable of providing a precise and accurate estimation of vitamin C, the related drawbacks cannot be disregarded when the ultimate goal of an ideal method is being considered. Due to the lack of specificity to vitamin C, some of these methods are inappropriate in the presence of other reducing agents.[35] Some methods display drawbacks in terms of cost effectiveness.[31] The crucial weakness of all these methods is its inability to quantify vitamin C at low analyte concentration,[36] thus restricting its execution in pharmaceutical and food industry as well as its biological evaluation which entails trace analyses. Though electrochemical analysis is one of the prominent techniques in the present scenario for the detection of vitamin C under dilute conditions, it is also not free from flaws. The major drawback of this method is the high over potential which causes the fouling occurred by the adsorption of the oxidation products on the electrode surface and thus decreases the reproducibility and sensitivity of the electrode.[30] On the background of high industrial demand for an appropriate analytical system capable of fast, sensitive, selective, accurate, miniaturisable and low-cost assessment of vitamin C at analyte concentration as low as possible, research is still ongoing to meet the requirements for devising an ideal commercial sensor. The numerous research articles on vitamin C sensing in recent years rationalise the above statement and the present study is an attempt to address the quandary based on ceria nanoparticles.

The major challenge in implementing ceria as a sensor for an extremely water soluble molecule like vitamin C is its inherent hydrophobicity. In the absence of any chemical modification, surface of ceria is hydrophobic due to their unique electronic structure which prevents it from hydrogen bonding with interfacial water.[37] Herein we have adopted a bilayer surface modification using oleic acid to render surface of ceria nanoparticles hydrophilic. The as synthesised water dispersible nanoparticles exhibited green coloured fluorescence in connection with its ultrafine size and its realistic perspective as a vitamin C sensor by modulating the Ce^{3+} content have been demonstrated. To date, there is only one study exploring the capability of ceria for sensing vitamin C, thus justifying further research in this area. The study was conducted by Sharpe et al. and was based on the colorimetric change of ceria nanoparticle after its interaction with antioxidants.[38] The detection range was 20 to 400 mM implying its limitation to sense the molecule in dilute conditions which is highly desirable for its pharmaceutical estimation. Moreover, certain issues like selectivity have not been addressed in the context, causing concern on its practical applicability. The present work is expected to receive great attention due to the ease and efficiency of the method to sense vitamin C at a concentration as low as 6 μM with higher reproducibility, selectivity and rapidness. Besides, to the best of our knowledge, this is the first report to date, which projects ceria as a 'turn-on' fluorescent sensor by making use of its redox property.

Experimental

Materials and synthesis

All the chemicals were used as received without further purification. Cerium acetate (99.9%), the precursor used, ascorbic acid (99%), potassium permanganate (99%), citric acid anhydride (99%) and calcium carbonate (99%) were purchased from Merck (India), titanium dioxide (99%) was purchased from CDH Laboratory Reagents, India, D-glucose (> 99.5%),

View Article Online
DOI: 10.1039/C6RA07504E

diphenyl ether (99%) and oleyl amine (70%) were procured from Sigma Aldrich, oleic acid (90%) was obtained from Alfa Aesar (UK), ammonium hydroxide (25%, analytical grade) was brought from Qualigens Fine Chemicals, India. Common solvents such as acetone, cyclohexane and toluene (analytical grade) were acquired from Merck, India. Branded pharmaceutical formulations as well as supplements of vitamin C in the form of tablets have been supplied by Glaxo Smithkline Pharmaceuticals Limited, India and Wipro Care India, the amount of the vitamin in each tablet was 500 mg and 1 mg respectively. Double distillation water using a quartz glass distillation unit was utilised for the synthesis procedure.

Synthesis of oleophilic ceria nanoparticles

Size controlled synthesis of cerium oxide was carried out by executing a thermal decomposition method. The precursor, cerium acetate, dissolved in diphenyl ether solvent (boiling point ~260 °C), upon supply of heat, will undergo decomposition to form the corresponding oxide. Oleic acid, by virtue of the steric effect provided by its long alkyl chain, was used as a surfactant to control the size of the nanocrystals. In a typical synthesis, 0.005 mole of cerium acetate was dissolved in 100 ml diphenyl ether in a round bottom flask. About 0.02 moles oleic acid and 0.023 moles oleylamine were added to the reaction mixture and were refluxed at its natural boiling point for 1 h. Oleic acid, in the presence of oleyl amine, undergoes ionisation to form the corresponding oleate ion which is capable of coordinating with the positive core of the nanoparticles formed. As the reaction progresses, the solution turned brown, indicating the formation of ceria crystals. The mixture was allowed to cool to room temperature, 1 h, after commencing the thermal decomposition. Acetone was added to the reaction mixture to precipitate the oleic acid coated nanoparticles, which were later separated by centrifugation. The separated nanoparticles were washed thoroughly with acetone to remove excess oleic acid and finally dried in an air oven to obtain a pale brown powder which is denoted as MLNP. The successful surface modification was confirmed by dispersing the nanoparticles in toluene, which yielded a transparent and stable dispersion.

Bilayer surface functionalisation of the oleophilic ceria nanoparticles

Oleic acid was again employed as a secondary surfactant to provide a bilayer coating over the nanoparticles. About 1 g of MLNP was combined with 20 ml of distilled water, which was almost immiscible, due to the hydrophobic nature of the NP surface. 20 ml of 10% (w/v) ammonium oleate in water was added drop-wise to this and stirred vigorously. Ammonium oleate was prepared by adding adequate amount of ammonium hydroxide to oleic acid so that the pH of the resultant solution is about 9, which is mandatory for the ionisation of oleic acid. After stirring the initial mixture of nanoparticle and oleate salt in water for about 3 h, mixture transformed into a stable suspension signifying the bilayer surface modification of oleate ions over the nanoparticle surface. The water in the suspension was allowed to evaporate slowly by providing a consistently boiling water bath as heat source. The nanoparticles obtained were washed thoroughly with cyclohexane, followed by acetone to remove any uncoated particles as well as unreacted oleate ions, which were later, dried and redispersed in water to yield a stable dispersion. The sample is named as BLNP henceforth.

Preparation of ceria dispersions for sensing vita-min C under different concentrations

A parent dispersion of the nanoparticles in water has been prepared with a concentration of 0.0008 M, the photoluminescence spectra of which is recorded. To 2 ml of this dispersion, different volume (0.1 ml to 0.5 ml) of 0.5 mM potassium permanganate solution was added and its photoluminescence was continuously monitored to optimise the volume of permanganate solution required to quench its fluorescence. A set of vitamin C solutions in water at concentrations in the range of µM to mM have been prepared and 2 ml of each solution was added to 2 ml of the ceria dispersion whose fluorescence has been quenched by the addition of permanganate. The quantitative estimation of vitamin C has been carried out by the acquisition of the photoluminescence spectra of the respective samples. For demonstrating the selectivity of the sensor towards vitamin C, different concentrations of common pharmaceutical ingredients such as citric acid, calcium hydroxide, glucose and titanium dioxide in water have been added to BLNP dispersion and the PL spectra of the same was acquired. For the analysis of commercial samples, the tablets under study were dissolved in water so that its concentration falls in the µM range and 2 ml of this solution was mixed with 2 ml of the fluorescence quenched BLNP dispersion, whose photoluminescence intensity was also acquired.

Instrumental Techniques

The X-ray diffraction (XRD) patterns of the powder specimens were obtained using a Philips X'PERT PRO diffractometer with Ni-filtered CuKα1 radiation (λ = 1.5406 Å) using 30 mA current at 40 kV. The continuous scan was performed in the 5-100 degree (2θ) range at a scanning speed of 2 degree per min and a step size 0.04°. The thermogravimetric analysis (TGA) of the powders were carried out using a Perkin Elmer, STA 6000 simultaneous DTA-TGA in ambient atmosphere heated at a constant ramp of 10 °C min^{-1} under air purge. The morphology and average size of the nanocrystals were investigated by high resolution transmission electron microscopy (HR-TEM) using a FEI Tecnai 30 G2 S–Twin microscope operated at 300 kV and equipped with a Gatan CCD camera. The zeta potential as well as size of the cerium oxide nanoparticles in the suspension were carried out by photon correlation spectroscopy (PCS) at 25°C on a Zetasizer 3000 HSA, Malvern Instruments, Worcestershire, UK using a 60 mW He–Ne laser producing 633 nm wavelength with General Purpose algorithm with Dispersion Technology Software (v. 1.61) at 90° detection angle. A minimum of seven measurements for each sample were taken to ensure statistical significance. The water contact

View Article Online
DOI: 10.1039/C6RA07504E

angle measurements were made on glass substrates coated with aqueous and nonaqueous nanoparticle dispersions of same concentration by sessile drop method in a Data Physics DCAT21 Dynamic Contact Angle Meter which is equipped with a contact angle goniometer and high resolution cameras and software to capture the profile of a pure liquid on a solid substrate. A micro syringe steel needle (Hamilton) of capacity 500 µL was positioned above the surface of the coated glass slide, and a drop of the test liquid (3 µL) was dispensed at a rate of 1 µL s^{-1}. After dispensing the drop, its shape was monitored with a digital camera, and the contact angle was determined by aligning the tangent of the sessile drop profile at the contact point with the surface. The angle formed between the liquid/solid interface and the liquid/vapour interface is the contact angle and was an average of 5 measurements. The colloidal stability of the nanoparticle dispersion was monitored with a nephelometer (CL 52D, ELICO, India) as intensity of transmitted visible light through the fluid against time. The absorption spectra of the samples were obtained using a UV–visible 2401 PC spectrophotometer (Shimadzu, Japan) in the wavelength range 200–800 nm. The photoluminescence (PL) spectra of the nanoparticle dispersions (MLNP in toluene and BLNP in water) were taken at room temperature using a Cary Eclipse spectrofluorometer (Varian, Australia) with an excitation wavelength of 400 nm, unless otherwise specified. For each measurement, three replicates were carried out and the final value was represented in terms of standard deviation of the replicates. X-ray photoelectron spectroscopy (XPS) spectra of the particles powders were recorded on a VG Microtech Multilab ESCA 3000 spectrometer, maintaining a base pressure of the analysis chamber in the range of 3−6×10−10 Torr. Mg Kα (1253.6 eV) was used as the X-ray source. Binding energy (BE) calibration was performed with Au 4f7/2 core level at 83.9 eV. The XPS data was deconvoluted with XPSPEAK 4.1 software which produced stable and almost super imposable baselines, confirming the stability of the fits and helping to validate the interpretation.

Results and discussion

Synthesis and surface functionalisation of nano-particles

Cerium oxide nanoparticles were prepared by thermally decomposing cerium acetate in diphenyl ether at 260 °C, which is the natural boiling point of the sol-vent. The choice of the synthetic strategy is ingrained on its ability to produce highly crystalline and monodisperse nanoparticle compared to other methods.[39] As already reported, the decomposition of cerium acetate proceeds via the formation of free radical intermediates, as shown in equations below.[40]

$$M–OOCR \rightarrow M^{\bullet} + R–COO^{\bullet} \quad (1)$$
$$M–OOCR \rightarrow MO^{\bullet} + R–CO^{\bullet} \quad (2)$$
$$M^{\bullet} + MO^{\bullet} \rightarrow M–O–M \quad (3)$$

The association between $Ce^{\bullet}$ and $CeO^{\bullet}$ free radicals resulted in Ce–O–Ce linkage, which ended up with the nucleation of CeO_2 crystals.[40] The function of the surfactant, oleic acid is to control the growth of nanocrystals after nucleation and thus ensuring the ultra fine dimension of the formed nanoparticles. The oleate ions formed due to the ionisation of oleic acid in the presence of oleyl amine, possess a negatively charged head, corresponding to the carboxylate group and a non-polar tail comprising of the longer alkyl chain.[28] During the course of the reaction, the negative oleate head gets attached to the nucleated metal oxide core, which is usually positive in nature.[41] According to previous studies, restriction in crystal growth, imparted by the bulky as well as the kinked structure of oleic acid triggers the size controlled formation of nanoparticles.[42] The particular mode of attachment of oleate ion with the nanoparticle resulted in the protrusion of non-polar alkyl chain over the particle surface, thus inducing hydrophobicity on its surface. As the as prepared nanoparticle dispersibility is limited to organic solvents, their incompatibility with water is in turn, a hurdle for applications intended on aqueous media. In order to make the particles attuned to hydrophilic surroundings, slight polarity has been induced over the surface of nanoparticles by oleic acid mediated bilayer surface encapsulation. The conceptual pathway of the synthetic strategy has been depicted in Scheme 1.

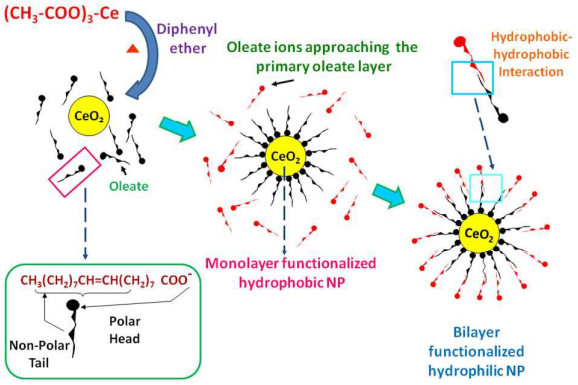

Scheme 1 Synthetic protocol for the bilayer surface functionalised hydrophilic nanoparticles.

The long, non-polar alkyl chain of the oleate ion in the monolayer intertwines with that of the oleate ions which have been added during the bilayer surface modification process. This interlink has been effected by the hydrophobic-hydrophobic interaction among the two alkyl chain[43] which ultimately resulted in the projection of the carboxylate group of the oleate ion over the nanoparticle surface. The polarity brought about by the C–O− bond in the carboxylate ions reversed the characteristics of nanoparticle surface from hydrophobic to hydrophilic. The visual change in the appearance of the nanoparticles after bilayer modification has been depicted in Fig. S1 of Electronic supplementary Information. It could be observed that whereas MLNP had a sticky nature, BLNP was more powder like. This is an initial evidence for the change in the nanoparticle surface from hydrophobic to hydrophilic. The dispersibility of BLNP in water (Fig. S1) could be considered as a confirmation for the success of the synthetic strategy.

View Article Online
DOI: 10.1039/C6RA07504E

Preliminary Characterisation

The XRD patterns of BLNP shown in Fig. 1 reveals that the core of the nanoparticle belongs to pure face-centered cubic fluorite phase of ceria with the space group $Fm\bar{3}m$ (JCPDS no. 43-1002).[44] The characteristic peaks in the diffractograms has been indexed to the reflections from the crystal planes in the (111), (220), (311) and (331) directions as denoted in the figure.[45] The extremely broadened XRD peaks indicate the nanoscale of the crystallites and the D_{XRD} calculated using Scherrer equation is 1.6 nm.

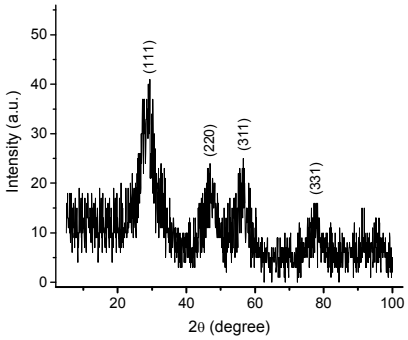

Fig. 1 X-ray diffraction patterns of BLNP showing the characteristics peaks corresponding to the crystal facets of ceria.

HR-TEM images of BLNP, as demonstrated in Fig. 2, vividly illustrate the spherical morphology of the particles and the calculated average size on 100 particles is 2.2±0.2 nm. The relatively low contrast in the TEM image of the crystal are apparently due to the presence of the surfactant, oleic acid over the surface of nanostructure.[28] The uniform size distribution and well separation among the particles without any apparent interaction as revealed by TEM is credited to the surface modification facilitated by oleic acid, thus substantiating its role in the size controlled synthesis. The visual examination of the exposed crystal facets of BLNP indicates that the lattice fringes corresponds to predominant (111) and (100) planes of ceria with corresponding interplanar spacing of 0.31 nm and 0.27 nm respectively, indicating the crystal purity of the core structure.

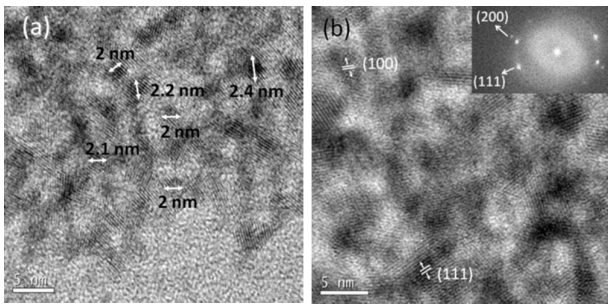

Fig. 2 HR-TEM images of BLNP (a) showing the size of particles (b) indicating the exposed facets of the crystal.

The hydrodynamic sizes of the particles in its aqueous (12.6 nm) as well as non-aqueous dispersion are showed in Fig. 3. The D_{PCS} value of the MLNP nanoparticles (4.5 nm) is slightly higher than the D_{TEM} and the difference is because, whereas D_{TEM} provides only the size of the core nanoparticle, D_{PCS} considers the size of the core-shell structure comprising of nanoparticle and the surfactant.[46] The value of D_{PCS} is in good agreement with D_{TEM}, when the chain length of the surfactant on the NP surface is considered.

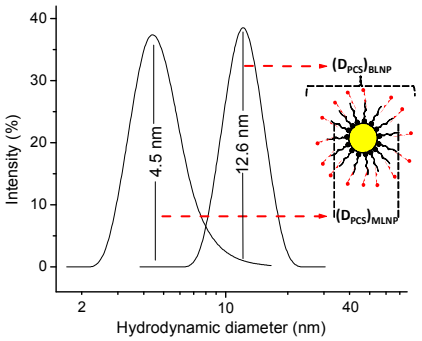

Fig. 3 The photon correlation spectra of MLNP and BLNP in toluene and water respectively for deriving its hydrodynamic diameter.

The D_{PCS} of the nanoparticle in aqueous dispersion (BLNP) was higher than that in non-aqueous dispersion and the increase is brought about by the double layer of oleic acid over the nanoparticle surface in the aqueous media compared to the monolayer of surfactant in oleophilic MLNP.

Surface properties of the nanoparticles

The thermogravimetric profiles of the samples and the zeta potential of the aqueous BLNP dispersion (pH~7) are shown in Fig. 4. Panel A shows significant decrease in weight between 240 to 450 °C on account of the removal of surfactants from the surface of the nanoparticle. MLNP showed a single step weight loss corresponding to the monolayer chemisorbed oleate ions over the nanoparticles.

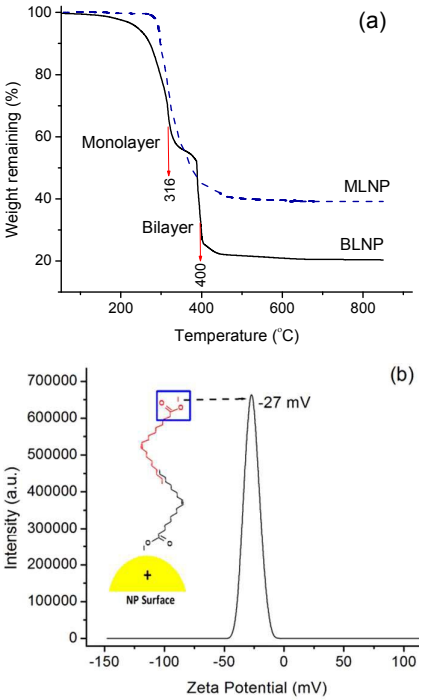

Fig. 4 (a) The thermogravimetric profiles of MLNP and BLNP, and (b) zeta potential measurement of BLNP in water.

View Article Online
DOI: 10.1039/C6RA07504E

The bilayers of surfactant in BLNP resulted in a two step weight loss in its thermal stability data, the first and the second step being related to the outer and inner layers respectively. As the outer layer is linked to the inner layer by relatively weak hydrophobic-hydrophobic interaction due to partial interpenetration of the hydrocarbon tails, the oleate ions in that layer could get rid of the attractive force and undergo decomposition at a lower temperature (316 °C) compared to that in the inner layer (400 °C). In the primary layer, owing to the strong chemisorption between the oleate ions and the nanoparticle surface, the surfactant molecules undergo decomposition at a slightly higher temperature as implied by the TGA. In fact, the two step weight loss in BLNP implies the effectiveness of surface functionalisation proffered by the adopted synthetic strategy. In order to evaluate the surface charge of the particles after bilayer surface functionalisation, the zeta potential of the aqueous BLNP dispersion (pH ~7) has been measured (Fig. 4, panel b). The particles show a negative zeta potential of about –27 mV which is attributed to the negative carboxylate groups projecting out of the nanoparticle surface after bilayer modification. The value, which in turn implies the polarity over the surface, confirms the successful grafting of hydrophilic layer over the nanoparticles by functionalisation.

The change in the nature of the nanoparticles from hydrophobic to hydrophilic has also been demonstrated in Fig. 5 which reveals the water contact angle measurements of glass slides coated with dispersions of MLNP and BLNP. The wetting behaviour exhibited by the particles before and after bilayer functionalisation is drastically different. Whereas MLNP coated surface made a contact angle of 97° with water which falls in the hydrophobic range, glass slide with BLNP over the surface exhibited a hydrophilic contact angle of 50°. The difference in wettability of the two samples is featured by the change in the functional groups over the nanoparticle surfaces brought about by surface modification. In MLNP, due to the non-polar hydrocarbon chain over the nanoparticle, the surface is rather hydrophobic as shown in Fig. 5a.

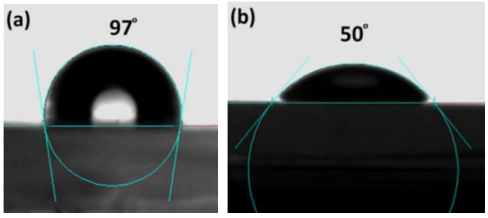

Fig. 5 Sessile drop water contact angle measurement of glass slide coated with (a) MLNP and (b) BLNP.

On the other hand, the surface polarity of BLNP as endowed by the carboxylate group, due to the reverse manner of attachment of the alkyl chains among each other in the two layers, rendered the glass surface hydrophilic. The hydrophilic surface of nanoparticles facilitated its dispersion in water (Fig. S1) which were stable over a period of several weeks. The dispersion did not show any visible change in appearance or formation of precipitate over the time of ageing. The zeta potential value of the dispersion, –27 mV also indicates the stability of the dispersion, as the values in the range 25–30 mV specifies the electrostatic stabilisation of the nanoparticles.[47]

Table 1 Turbidity Measurement data of BLNP aqueous dispersion

Ageing Time (Days)	Turbidity (NTU)	Decrease in turbidity (%)
1	22	0
7	19	19
14	19	13
21	19	13
28	19	13
35	19	13

The turbidity measurement of the dispersion for more than 1 month is presented in Table 1. Though, the initial value of the turbidity i.e., 22 NTU slightly decreased to 19 NTU after 1 week, later, the dispersion showed no further precipitation for more than 1 month. Thus the turbidity data, along with the zeta potential of the dispersion corroborates the higher stability offered by the hydrophilic nanoparticles in water.

Optical properties of the nanoparticles

The absorption and emission spectra of BLNP is depicted in Figure 6. The particles showed its absorption edge at 400 nm and the corresponding emission was in the visible region with its emission maximum at 515 nm which is in the green region. Ceria usually absorbs in the UV region on account of the charge-transfer transition from O_2 (2p) to the Ce^{4+} (4f) orbital.[16] Hence, the optical properties of BLNP shows a red shift with respect to bulk ceria towards visible region. Ultra fine ceria was already reported to show a size related red shift in absorption and associated green coloured emission.[28] The red shift is attributed to the higher amount of Ce^{3+} in the crystals associated with the high surface to volume ratio.

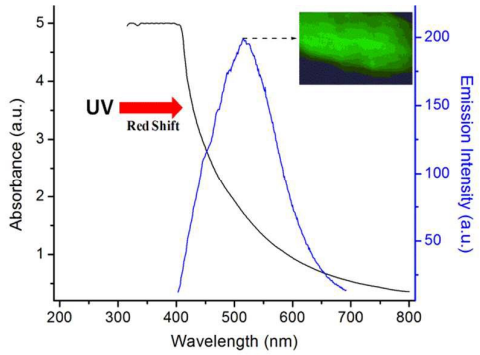

Fig. 6 Absorption and emission spectra of aqueous dispersion of BLNP showing a redshift from the UV region. The inset shows the visual image of the green coloured emission.

In ceria, the surface entropy of Ce^{3+} ions is higher than that of the bulk which persuades most of the surface atoms to exist in +3 oxidation state. With increase in surface area, there will be a subsequent increase in Ce^{3+} to Ce^{4+} ratio. The Ce^{3+} ions in the crystal lattice create an intermediate band in between the valence and conduction bands of ceria. As a result, the excitation of electrons from valence band occurs to this new band which is of lower energy than the conduction band. Thus the overall energy of absorbance was lowered to bring up a red shift in optical properties. Consequently, the absorption edge of BLNP is shifted to 400 nm

View Article Online
DOI: 10.1039/C6RA07504E

with a strong emission in the visible region. Thus the size dependent green coloured fluorescence exhibited by the particles is due to the presence of Ce^{3+} in the crystal. The higher Ce^{3+} content of ~38% as revealed by the XPS spectra of BLNP (Fig. S2) apparently supports the proposed conjecture.

Sensing of vitamin C by the nanoparticles

With respect to the optical properties of the nanoparticles, the role of Ce^{3+} is pivotal in the fluorescence exhibited by the nanoparticles. The dependence of fluorescence on the Ce^{3+} content has been verified by monitoring the emission intensity of the nanoparticles at various Ce^{3+} concentrations. Being an oxidising agent, $KMnO_4$ has been used as a mediator to vary the amount of Ce^{3+} in BLNP dispersion. $KMnO_4$ converts Ce^{3+} to Ce^{4+} according to the equation[48]

$$3Ce^{3+} + MnO^{4-} + 2H_2O \rightarrow 3Ce^{4+} + Mn^{4+} + 4OH^- \quad (4)$$

Different amounts of 0.0005 M $KMnO_4$ were added to BLNP dispersions, the PL spectra of which are shown as Fig. 7. It is observed that, the PL spectra showed a relative decrease in intensity with respect to the amount of $KMnO_4$ added. On the basis of available literatures mentioning the role of Ce^{3+} in the fluorescence property of ceria,[28,49,50] it could be assumed that, as Ce^{3+} is oxidised to Ce^{4+} by $KMnO_4$, the abundance of the intermediate energy level created by Ce^{3+} in the band gap will be inversely affected.

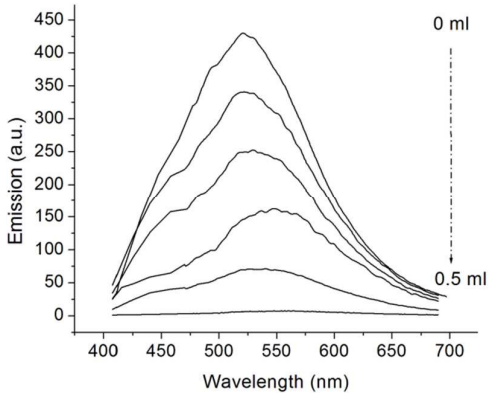

Fig. 7 The PL spectra of BLNP dispersion (in water) showing quenching of fluorescence with the addition of different volume of $KMnO_4$ solution.

The consequential decrease in exciton transfer to the Ce^{3+} band allocated the diminishing of fluorescence exhibited by the nanoparticles. The oxidation of Ce^{3+} to Ce^{4+} could also be observed visually by examining the colour change of the BLNP dispersion. The BLNP dispersion which was initially bluish-white in colour gradually changed to yellowish, after the addition of $KMnO_4$, indicating the formation of Ce^{4+} in the dispersion. The optical photograph of the dispersions before and after the addition of $KMnO_4$ has been supplied as Fig. S3. The amount of $KMnO_4$ needed to quench the fluorescence of BLNP dispersion under the preferred experimental conditions has been optimised to 0.5 ml (0.25 µmoles of $KMnO_4$), the addition of which extinguished the fluorescence of the nanoparticles almost completely.

The principle of the present nanoparticle based sensor is laid on the fact that the reverted conversion of Ce^{4+} to Ce^{3+} by vitamin C can fetch the extinct fluorescence to its initial vigour. The structure of vitamin C is such that the two enolic hydroxyl groups attached to the C3 and C2 carbon of the lactone ring are prone to release electron under favourable conditions so as to form the comparatively stable and oxidised deprotonated intermediate.[51] The sensing of vitamin C by nanoparticles stems from its the ability to convert the oxidised Ce^{4+} back to Ce^{3+} by the donation of electron as represented in Scheme 2. The stoichiometric equation displaying the interaction between vitamin C and cerium ions is shown as equation (5)[48]

$$2Ce^{4+} + \underset{\text{(Vitamin C)}}{C_6H_8O_6} \rightarrow 2Ce^{3+} + C_6H_6O_6 + 2H^+ \quad (5)$$

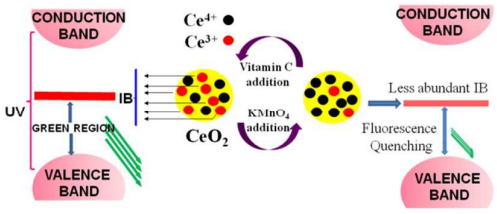

Scheme 2 Representation of the principle behind the sensing of vitamin C by ceria nanoparticles.

According to literature[28,49,50], as the creation of IB is based on the concentration of Ce^{3+}, we could propose that when Ce^{4+} is converted back to Ce^{3+}, the intermediate band (IB) in the band gap is regenerated, which establishes the initial fluorescence. Different amounts of vitamin C in water at concentrations in the range of µM to mM have been added to BLNP dispersions, whose fluorescence has been quenched by the oxidation of Ce^{3+}. Upon addition of vitamin C, the oxidised cerium ions (Ce^{4+}) will return to their initial +3 state along with the regain of the fluorescence, whose emission intensity is decided by the amount of vitamin C. The analysis of PL spectra of the respective dispersions in fact confirms that the intensity of emission by the nanoparticles is a function of the concentration of vitamin C present in the dispersion.

Variation in PL intensity of BLNP and the linear fit of the PL intensity plotted against the vitamin C concentrations at low concentration range are shown in Fig. 8. The PL intensity of the dispersion showed a linear correlation with the concentration of vitamin C. The linearity could be observed over a wide range of concentration of vitamin C solution (µM to mM). However, there is no observable increase in PL intensity upon addition of vitamin C solution with concentration above ~2.6×10^{-4} M. Here the noteworthy fact is that, at this concentration, the PL spectra have almost regained its initial intensity implying complete retrieval of Ce^{4+} to Ce^{3+}. The variation in PL intensity with the addition of ultra dilute vitamin C solution (µM) is perfectly linear as seen from the linear regression (panel b) with an R2 value of 0.9963. The linearity implies the efficiency of the proposed sensor to quantify vitamin C under ultra dilution. The limit of detection (LoD) of the sensor, which is smallest analyte concentration that can be measured reliably by the proposed method, has been calculated as 3 times the standard deviation (σ) for replicates of the blank.[48] A combination of very small scatter (σ), 0.17 and the ability to detect reproducibly at much lower concentration levels compared to that already

View Article Online
DOI: 10.1039/C6RA07504E

reported, positions our nanoparticles based sensor as very promising to estimate vitamin C in solutions as dilute as 500 nM.

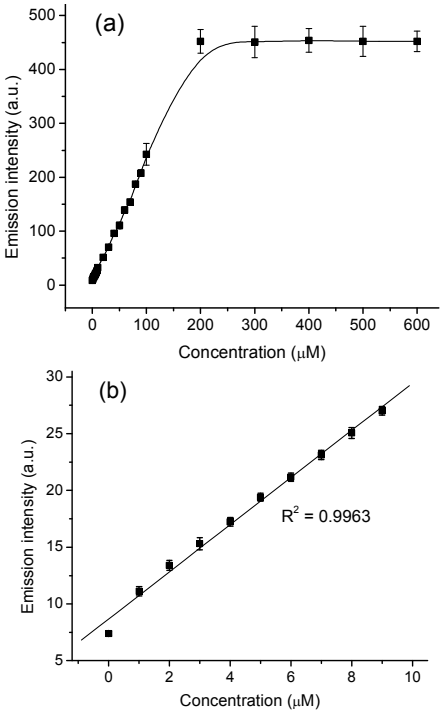

Fig. 8 (a) Variation in PL intensity of BLNP with the addition of different concentrations of vitamin C solution, and (b) linear fit of the PL intensity plotted against molarity of vitamin C at low concentration range.

In short, the dynamic range of detection of the sensor is assigned to be 10^{-7} to 10^{-4} M (0.02 to 17.6 ppm).

The selectivity of the sensor towards vitamin C in pharmaceutical formulations and the response time of the sensor detecting vitamin C have been demonstrated in Fig. 9. Common pharmaceutical ingredients which are used as sweetening agents, stabilisers and binders have been employed along with BLNP and the PL spectra of the same was acquired. It was observed that almost all of the ingredients did not show any interaction with the nanoparticles so as to create any impact on its PL spectra. It is also revealed that any of the ingredients does not interfere with the interaction between vitamin C and the nanoparticles as implied by the retention of the linear progression of PL intensity with vitamin C concentration in the presence of all ingredients.

The selectivity of the sensor towards vitamin C in pharmaceutical formulations and the response time of the sensor detecting vitamin C have been demonstrated in Fig. 9. Common pharmaceutical ingredients which are used as sweetening agents, stabilisers and binders have been employed along with BLNP and the PL spectra of the same was acquired. It was observed that almost all of the ingredients did not show any interaction with the nanoparticles so as to create any impact on its PL spectra. It also revealed that any of the ingredients does not interfere with the interaction between vitamin C and the nanoparticles as implied by the retention of the linear progression of PL intensity with vitamin C concentration in the presence of all ingredients.

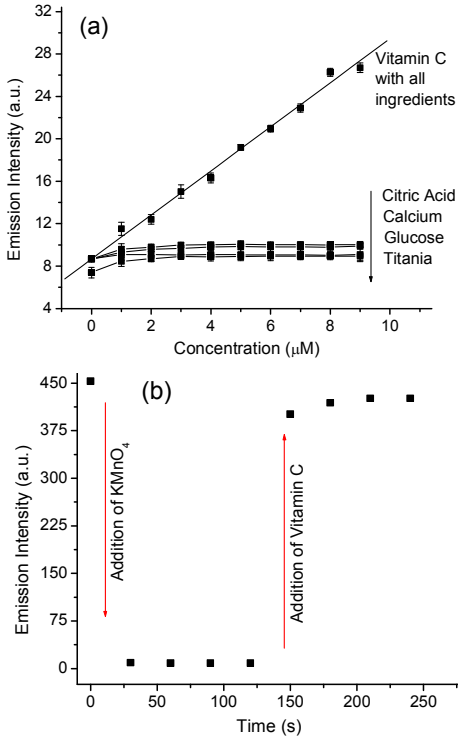

Fig. 9 (a) Variation in PL intensity of BLNP with the addition of different pharmaceutical ingredients at different concentrations. The same with the addition of vitamin C along with all ingredients is also shown and (b) time dependent variation in PL intensity of BLNP dispersion with the addition of KMnO4 and vitamin C.

The PL intensity of the dispersion as a function of time has been monitored and during the approach, the fluorescence was quenched and activated by the addition of $KMnO_4$ as well as vitamin C. It is noticed that the PL intensity which diminished by the addition of $KMnO_4$, could be resumed within 30 seconds after the addition of vitamin C (panel b of Fig. 9). In order to point up the reusability of the sensor, five consecutive additions of $KMnO_4$ followed by vitamin C addition was executed on the dispersion and the resultant PL intensity is featured in Fig. 10. The turn on/off behaviour of the nanoparticle emission intensity was retained even after 5 cycles without much difference in initial intensities.

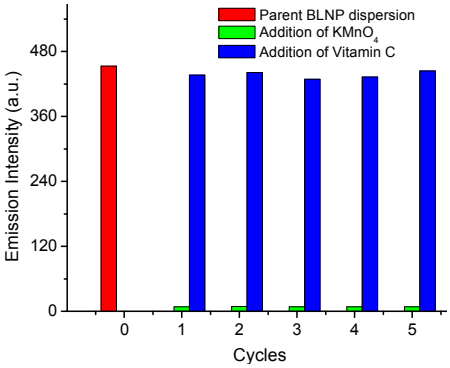

Fig. 10 Variation in PL intensity of BLNP with the alternate addition of $KMnO_4$ followed by vitamin C.

View Article Online
DOI: 10.1039/C6RA07504E

Thus the reversibility of fluorescence exhibited by the nanoparticles enhanced its long term usability, which is one among the prerequisites of a desirable sensor. Attempt has been made to elucidate the amount of vitamin C in some pharmaceutical formulations by means of the projected sensing procedure (see ESI). The results for the evaluation of vitamin C in real samples are tabulated in Table 2.

Table 2 Summary of the quantitative estimation of vitamin C in commercial samples

Sample	Certified amount of vitamin C per tablet (mg)	Evaluated amount of vitamin C per tablet (mg)	Recovery (%)	RSD (%)
Tablet 1	500	528	105	0.107
Tablet 2	1	0.98	98	0.092

The satisfactory RSD (relative standard deviation) and % recovery substantiates the reliable estimation of vitamin C in commercial formulations within acceptable error limits. Thus the practical applicability of the adapted method has been validated by the analysis of real samples. In short, without any tedious methodologies, expensive instrumentation or storage protocols, the presented method could rapidly and repeatedly sense vitamin C with high accuracy.

Conclusions

A novel turn–on fluorescent sensor based on cerium dioxide has been devised by a simple two step synthetic strategy. The principle of the sensor is relied on the redox property of ceria and its dependence on the size induced fluorescence. Nanoscale ceria with average size ~2.2 nm has been engineered by thermally decomposing cerium acetate in diphenyl ether in the presence of oleic acid as surfactant. The oleophilic surface of the as synthesised nanoparticles has been renovated to hydrophilic by imparting a bilayer surface functionalisation. The consequent change in its property was reflected in its surface polarity as well as wetting behaviour as revealed by the zeta potential and contact angle measurements. One of the appealing achievements of the demonstrated method is that, while the bilayer surface functionalisation allowed the surface of the particles hydrophilic, there was no inverse effect on the behaviour of the central ceria core including its optical and redox properties. The implemented hydrophilic features enabled the water compatibility of the nanoparticles to yield its aqueous dispersion, which exhibited long term stability. The emission intensity of the nanoparticles showed a quenching behaviour with respect to the oxidation of Ce^{3+} to Ce^{4+} in the nanoparticle dispersion by $KMnO_4$. The reversion of the oxidation state from Ce^{4+} to Ce^{3+} with the addition of vitamin C showed a linear increase in fluorescence intensity with its concentration, thus enabling its quantitative assessment. The fascination with the proposed method is its efficiency to sense vitamin C at a concentration as low as 500 nM with higher reproducibility, selectivity and rapidness, without any tedious protocol. The intriguing possibilities of the method for practical application have also been demonstrated by satisfactorily quantifying vitamin C in its commercial supplements with high accuracy.

Acknowledgements

The authors thank CSIR-NIIST for providing the necessary facilities for the work and the CSIR–Central Glass & Ceramic Research Institute for continuing the same. Miss. Srividhya J. Iyengar of CSIR-CGCRI, Kolkata is acknowledged for the XPS measurements. Mr. M. Kiran and Ms. Remya are acknowledged for HR-TEM imaging and zeta potential measurements. Authors gratefully acknowledge Dr. Sailaja G. S. of CUSAT, Dr. Prabha D. Nair and Ms. Nimi of SCTIMST for water contact angle measurements. Authors AK and TSS acknowledge CSIR for the CSIR Fellowships. This work was partly funded by the Indian Rare Earths Limited Technology Development Council (IRELTDC), DAE, India.

Notes and references

1 A. Ahniyaz, Y. Sakamoto and L. Bergstrom, *Cryst. Growth Des.,* 2008, **8**, 1798.
2 A. Trovarelli, C. de Leitenburg, M. Boaro and G. Dolcetti, *Catal. Today*, 1999, **50**, 353.
3 M.Yamashita, K. Kameyama, S. Yabe, S. Yoshida,Y. Fujishiro, T. Kawai and T. Sato, *J. Mater. Sci.*, 2002, **37**, 683.
4 H. Imagawa, A. Suda, K. Yamamura and S. Sun, *J. Phys. Chem.C,* 2011, **115**, 1740.
5 S. Deshpande, S. Patil, S. Kuchibhatla and S. Seal, *Appl. Phys. Lett.,* 2005, **87**, 133113.
6 C. Sun, H. Li and L. Chen, *Energ. Environ. Sci.,* 2012, **5**, 8475.
7 T. Garcia, B. Solsona and S. H. Taylor, *Catal. Lett.,* 2005, **105**, 183.
8 S. Maensiri, C. Masingboon, P. Laokul, W. Jareonboon, V. Promarak, P. Anderson and S. Seraphin, *Cryst. Growth Des.,* 2007, **7**, 950.
9 P. Palmisano, N. Russo, P. Fino, D. Fino and C. Badini, *Appl. Catal. B*, 2006, **69**, 85.
10 M. G. Bellino, D. G. Lamas and N. E. de Reca, *Adv. Funct. Mater.,* 2006, **16**, 107.
11 H. X. Mai, HL. D. Sun, Y. W. Zhang, R. Si, W. Feng, H. P. Zhang, H. C. Liu and C. H. Yan, *J. Phys. Chem. B,* 2005, **109**, 24380.
12 S.S. Lee, W. Song, M. Cho, H. L. Puppala, N. Phuc, H. Zhu, L. Segatori and V. L. Colvin, *ACS Nano,* 2013, **7**, 9693.
13 T. S. Sreeremya, A. Krishnan, K. C. Remani, K. R. Patil, D. F. Brougham and S. Ghosh, *ACS Appl. Mater. Interfaces,* 2015, **7**, 8545.
14 A. Younis, D. Chu, Y. V. Kaneti and S. Li, *Nanoscale,* 2015, **8**, 378.
15 S. M. Hirst, A.S. Karakoti, R. D. Tyler, N. Sriranganathan, S. Seal and C. M. Reilly, *Small,* 2009, **5**, 2848.
16 A. Corma, P. Atienzar, H. Garcia and J. Y. Chane-Ching, *Nat. Mater.,* 2004, **3**, 394.
17 S. Patil, S. Reshetnikov, M. K. Haldar, S. Seal and S. Mallik, J. *Phys. Chem. C,* 2007, **111**, 8437.
18 G. I. N. Waterhouse, J. B. Metson, H. Idriss and D. Waterhouse, *Chem. Mater.*, 2008, **20**, 1183.
19 S. Babu, J. H. Cho, J. M. Dowding, E. Heckert, C. Komanski, S. Das, J. Colon, C. H. Baker, M. Bass, W. T. Self and S. Seal, *Chem. Commun.*, 2010, **46**, 6915.
20 I. Celardo, J. Z. Pedersen, E. Traversa and L. Ghibelli, *Nanoscale,* 2011, **3**, 1411.
21 P. Jasinski, T. Suzuki and H. U. Anderson, *Sensor Actuat. B*, 2003, 95, 73-77.
22 S. Chakraborthy and A. Sen, *Sensor Lett.,* 2009, **7**, 91.
23 M. B. Gumpu, N. Nesakumar, S. Sethuraman, U. M. Krishnan and J. B. B. Rayappan, *Sensor Actuat*. B, 2014, **199**, 330.

View Article Online
DOI: 10.1039/C6RA07504E

24 M. Hosseini, M. R. K. Pur, P. Norouzi, M. R. Moghaddam, F. Faridbod, M. R. Ganjali and J. Shamsi, *Anal. Method*., 2015, **7**, 1936.
25 M. Singh, N. Nesakumar, S. Sethuraman, U. M. Krishnan and J. B. B. Rayappan, *J. Colloid Interf. Sci.*, 2014, **425**, 52.
26 D. Zhang, W. Wu, X. Ni, X. Cao, X. Zhang, X. Xu, S. Li, G. Han, A. Ying and Z. Tong, *J. Mater. Sci.* 2009, **44**, 3344.
27 S. H. Yu, H. Colfen and A. Fischer, *Colloids Surf. A*, 2004, **243**, 49.
28 A. Krishnan, T. S. Sreeremya, E. Murray and S. Ghosh, J. *Colloid Interf. Sci.,* 2013, **389**, 16.
29 A. Barberis, G. Bazzu, G. Calia, G.M. G. Puggioni, G. G, Rocchitta, R. Migheli, M. Schirra, M. S. Desole and P. A. Serra, *Anal. Chem*., 2010, **82**, 5134.
30 S. N. Faisal, M. M. Hossain and H. J. Lee, *J. Electrochem. Sci. Technol.,* 2010, **1**, 121.
31 Z. Gazdik, O. Zitka, J. Petrlova, V. Adam, J. Zehnalek, A. Horna, V. Reznicek, M. Beklova and R. Kizek, *Sensors,* 2008, **8**, 7097.
32 Y. T. Chen, F. A. Isherwood and L. W. Mapson, *Biochem. J.,* 1953, **55**, 821.
33 H. Beitollahi, A. Mohadesi, M. Mostafavi, H. Karimi-Maleh, M. Baghayeri and A. Akbari, Ionics, 2013, **20**, 729.
34 S. S. Mitic, D. A. Kostic, D. C. Naskovic-Dokic and M. N. Mitic, *Trop. J. Pharm. Res.,* 2011, **10**, 105.
35 P. J. O'Connell, C. Gormally, M. Pravda and G. G. Guilbault, *Anal. Chim. Acta,* 2001, **431**, 239.
36 Y. Andreu, S. de Marcos, J. R. Castillo and J. Galban, Talanta, 2005, **65**, 1045.
37 G. Azimi, R. Dhiman, H. M. Kwon, A. T. Paxson and K. K. Varanasi, *Nat. Mater.,* 2013, **12**, 315.
38 E. Sharpe, T. Frasco, D. Andreescu and S. Andreescu, *Analyst,* 2013, **138**, 249.
39 Y. W. Jun, J. S. Choi and J. Cheon, *Angew. Chem. Int. Edit.,* 2006, **45**, 3414.
40 T. S. Sreeremya, A. Krishnan, A. P. Mohamed, U. S. Hareesh and S. Ghosh, *Chem. Eng. J.*, 2014, **255**, 282.
41 S. Y. Lee and M. T. Harris, *J. Colloid Interf. Sci.,* 2006, **293**, 401.
42 A. Krishnan, T. S. Sreeremya and S. Ghosh, *CrystEngComm,* 2015, **17**, 7094.
43 L. F. Shen, P. E. Laibinis and T. A. Hatton, *Langmuir*, 1999, **15**, 447.
44 P. Maitarad, D. Zhang, R. Gao, L. Shi, H. Li, L. Huang, T. Rungrotmongkol and J. Zhang, *J. Phys. Chem. C*, 2013, **117**, 9999.
45 M. Mari, B. Mueller, K. Landfester and R. Munoz-Espi, *ACS Appl. Mater. Interfaces,* 2014, **7**, 10727.
46 T. S. Sreeremya, K. M. Thulasi, A. Krishnan and S. Ghosh, *Ind. Eng. Chem. Res.*, 2012, **51**, 318.
47 M. Bloemen, W. Brullot, L. Tai Thien, N. Geukens, A. Gils and T. Verbiest, *J. Nanopart. Res.,* 2012, **14**, 1100.
48 W.Di, N. Shirahata, H. Zeng and Y. Sakka, *Nanotechnology*, 2010, **21**, 365501.
49 X. H. Lu, X. Huang, S. L. Xie, D. Z. Zheng, Z. Q. Liu, C. L. Liang and Y. X. Tong, *Langmuir*, 2010, **26**, 7569.
50 P. Patsalas, S. Logothetidis and C. Metaxa, *Appl. Phys. Lett*. 2002, **81**, 466.
51 R. P. Tripathi, B. Singh, S. S. Bisht and J. Pandey, *Curr. Org. Chem.*, 2009, **13**, 99.

View Article Online
DOI: 10.1039/C6RA07504E

Graphical Abstract

Size-Tuned Hydrophilic Cerium Oxide Nanoparticles as a 'Turn-on' Fluorescent Sensor for the Rapid Detection of Ultralow Concentration Vitamin C.

Asha Krishnan, Thadathil S. Sreeremya and Swapankumar Ghosh*

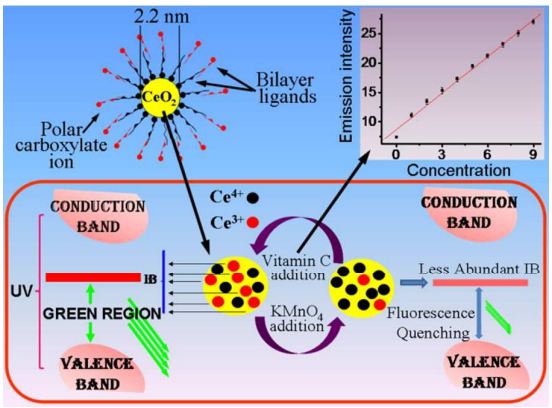

Hydrophilic ceria nanoparticles fabricated via bilayer surface functionalization approach shows tunable redox property depending on the Ce^{3+} content. The variation in the optical behaviour of the nanoparticles with Ce^{3+} content has been utilised as an analytical method to sense vitamin C with higher reproducibility, selectivity and rapidness under dilute conditions.